Design Optimization of a Manipulator for CERN's Future Circular Collider (FCC)

Hannes Gamper[1,2][a], Hubert Gattringer[2][b], Andreas Müller[2][c] and Mario Di Castro[1][d]

[1]*BE-CEM-MRO, CERN - European Organization for Nuclear Research, Espl. des Particules 1, 1211 Meyrin, Switzerland*
[2]*Institute of Robotics, Johannes Kepler University, Altenbergerstraße 69, 4040 Linz, Austria*

Keywords: Design Optimization, Redundant System, Manipulator.

Abstract: CERN is often confronted with very specialized automation problems in hazardous, radioactive and semi-structured environments for its particle accelerators, test rigs or other experiments. These frequently lead to specific requirements that do not allow the usage of common industrial robots. Thus, a design problem with almost no restrictions on the actual robot topology, but very hard requirements concerning workspace, allowed robot space, payload, robot weight and accuracy (due to elasticity/error propagation) has to be solved. This paper reports an approach to this problem, which was applied to find an optimal robotic design for inspection and maintenance tasks in CERN's Future Circular Collider (FCC).

1 INTRODUCTION

Since being founded in 1954, CERN - European Organization for Nuclear Research has been a continuously successful institution for particle physics, contributing major steps to complete the Standard Model of Particle Physics. The consecutive particle accelerators PS (Proton Synchrotron), SPS (Super Proton Synchrotron) and LHC (Large Hadron Collider) with their increasing center of mass collision energy of 50 GeV, 900 GeV and 14 TeV and corresponding increase in circumference of 628 m, 6.9 km and 27 km, were directly related to the award of the Nobel Prize in 1979 (PS), 1984 (SPS) and 2013 (LHC). The latter nobel prize was related to the discovery of the Higgs-Boson, which was predicted almost 50 years before its detection at CERN by Peter Higgs and thus completed the most precise model of our universe so far, the Standard Model of Particle Physics.

Yet, there are still phenomena, like dark matter, the prevalence of matter over antimatter or the neutrino mass, which cannot be described by the Standard Model. This suggests, that there must be more, physics which goes beyond the Standard Model and still has to be discovered. A good chance to unveil

---

[a] https://orcid.org/0000-0001-5522-734X
[b] https://orcid.org/0000-0002-8846-9051
[c] https://orcid.org/0000-0001-5033-340X
[d] https://orcid.org/0000-0002-2513-967X

such behavior is thought to lie in particles with a mass above 14 TeV and thus unable to be created by the current machines at CERN. To unlock observations in these high energy ranges, a new particle accelerator with a center of mass energy of 100 TeV and a circumference of 100 km was suggested: the Future Circular Collider - FCC.
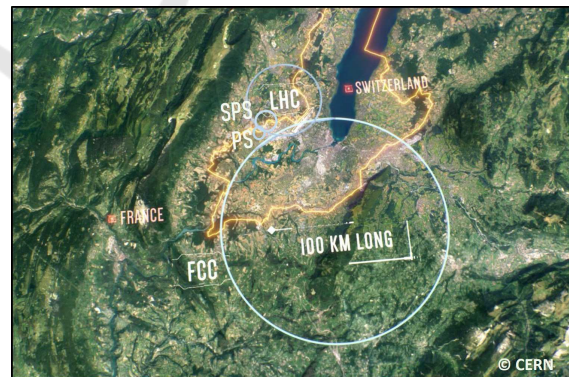

Figure 1: PS, SPS, LHC and FCC comparison.

In 2013 the European Strategy for Particle Physics initiated a Conceptual Design Report and feasibility study on the FCC. Since then numerous physics studies about possible future discoveries, the most promising energy ranges and the underlying theories, as well as engineering studies about possible construction sites, logistics, material research, automa-

tion techniques and socio-economic studies looking at the impact of a 9 GCHF science project in the middle of Europe, were conducted in collaborations of over 150 universities and finally published in 2019 within the Conceptual Design Report for a Lepton (FCC-ee) and Hadron (FCC-hh) Collider in (CDR, 2019a) and (CDR, 2019b). The 2020 Update of the European Strategy for Particle Physics listed the further investigation of the FCC as one of three main priorities and thus launched a Technical Design Report.

At this stage, in-depth studies like geodetic measurements for possible placements of the tunnel, structural simulations, material handling during construction, power supply, emergency scenarios and many more are conducted to estimate feasibility, cost and construction time. One of these studies concerns the automation of maintenance, inspection and emergency handling along the 100 km long FCC tunnel. The automation of these tasks plays a significant role for downtime, reliability and safety of particle accelerators and decreases the radiation exposure of workers. Since these tasks require various adept mechanical interactions with its environment in a huge work space, the study suggested a rail-based robotic system with a highly redundant manipulator for the FCC tunnel.

Based on this suggestion for a generic robot layout, this paper presents the applied methods to find a robot design with low production costs, low robot weight and lowest possible energy consumption, while providing the required precision. Furthermore the robot needs to perform most diverse kinds of operations from maintenance over inspection to emergency handling, while moving in the complex environments of the FCC-ee and FCC-hh tunnels.

In section **2** the environment, given tasks and derived requirements are presented. Some assumptions and an initial, tentative robot topology are shown in section **3**. Section **4** describes the modelling of the robot, optimization techniques and objectives as well as the final optimal robot topology. Then, in section **5** the prototype for future proof of concept studies is presented and the last section **6** discusses the conclusions drawn from this work.

2 ENVIRONMENT & TASKS

The FCC tunnel will have an inner diameter of 5.5 m and host two different configurations, first a lepton collider (the FCC-ee) and then a hadron collider (the FCC-hh) shown in figures 2 and 3, respectively.

The upper section **A** of the tunnel is separated by the ceiling **B** and will be used for smoke and he-

lium extraction in case of emergencies. The ceiling **B** will also function as the support structure for the rail-based robotic system. Several fire doors divide the tunnel into about 400 m long sections, through which the robot can pass via automated hatches. Thus, the robot space is limited to the area **C**, when traveling along the tunnel axis. Further installation material **D** like cable trays, fiber optics, helium recovery, compressed air and water pipes are placed on the left and right side of the cross-section. The floor **G** consists of reinforced concrete and embeds a fresh air duct **H** and a water drain **I**. The FCC-ee layout furthermore contains the booster ring **E** and the e+/e- ring **F** and the FCC-hh layout the cryostat **J** and the cryogenic distribution line **K**.
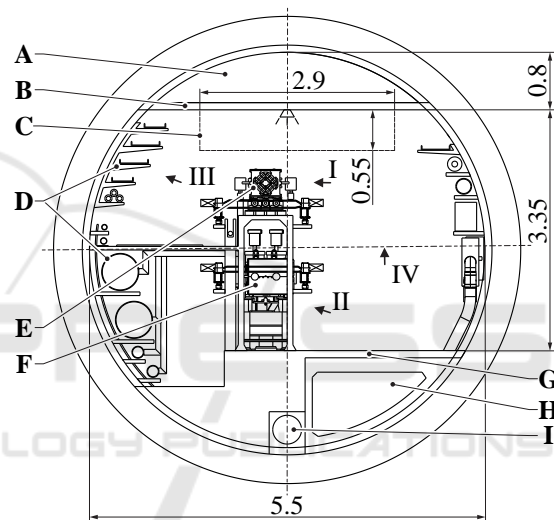

Figure 2: Cross-section FCC-ee.

In these environments the robotic system has to be able to handle different maintenance and inspection tasks. This requires the robot to reach a specific position and orientation (indicated with arrows in figures 2 and 3) while providing the necessary precision. The most diverse tasks, based on experience from interventions in the LHC, are:

- **BLM Inspection (I):** The Beam-Loss-Monitor sensors, described in (Holzer et al., 2012), on the right and left side of **E** and **J**, detect the loss of particles of the beam. These sensors need to be tested regularly by approaching them with a radioactive source while reading the sensor values.

- **Vacuum Leak Detection (II):** Loss of the vacuum in the cryostats can lead to fatal destruction, see incident in 2008 (M. Bajko, 2009). In case the vacuum pumps detect a leak, the robot has to move to the corresponding section and inject he-
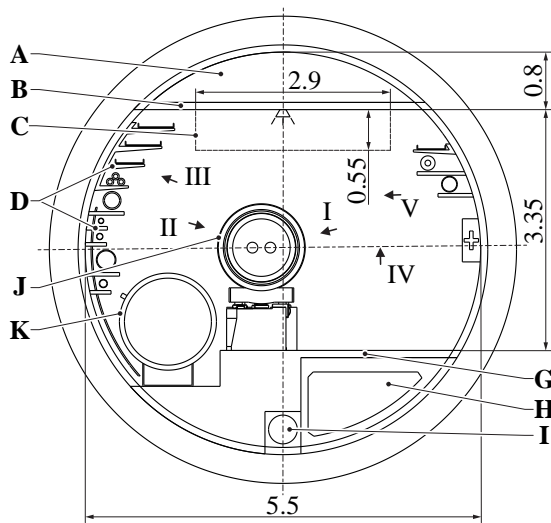
Figure 3: Cross-section FCC-hh.

lium at critical parts of the installation. Once the vacuum pumps detect helium, the location of the leak can be narrowed down until it is found.

- **General Exceptional Inspections (III):** In case of exceptional problems like failure of certain systems of the complex installations, the robot needs to inspect the tunnel immediately and save workers from possible hazards.

- **Radiation Measurement (IV):** Before workers are allowed in the tunnel after a shut down of the machine, the radiation levels along the tunnel axis will be measured, recorded and analyzed. Related systems in the LHC are presented in (Castro et al., 2018).

- **Alignment Measurement (V):** The cryostats, **E** and **J**, need to be aligned with high precision, to avoid potential beam loss. The alignment process and algorithms are described in (Missiaen et al., 2009) and (Valentino et al., 2012). To measure the alignment, a system of fiducials on the cryostats has to be detected and the relative position between consecutive elements will be measured, see (Bestmann, 2008).

The points discussed above give rise to certain requirements and restrictions, which are relevant for the topology of the robotic system:

1. A workspace of 5.5×3.35 m along the 100 km long tunnel.

2. Pass through fire door hatches with dimensions of 2.9×0.55 m.

3. Reach necessary positions according to the tasks.

3 MANIPULATOR DESIGN CONCEPT

The aim is to find the best-suited manipulator, based on the recommendation for a rail-based robotic system with a highly redundant manipulator by the conducted survey and the requirements and restrictions discussed in section 2. The manipulator is conceptually split up into a positioning mechanism (section 3.1) and a subsequent dexterous arm (section 3.2). The positioning mechanism serves to position and align the arm within the FCC tunnel. The dexterous arm will enable the robot to perform complex handling tasks while avoiding obstacles.

3.1 Positioning Mechanism

The topology of the first four joints was rather obvious and could be found by a manual exploration of possible joint configurations. Figure 4 shows the possible variants Vi for each of the four joints $J1$ to $J4$. The following enumeration discusses the pros and cons of the different variants for each joint:

1. Joint 1 in figure 4, implements a linear movement in direction of the tunnel axis (y-axis) according to the recommendation of a rail-based system.

2. Joint 2 spans the xy-plane by either introducing another linear movement in x-direction ($J2V1$) or a rotation around z-axis including an offset for the following robot link ($J2V2$). $J2V1$ requires less space and will increase the dexterity of the manipulator.
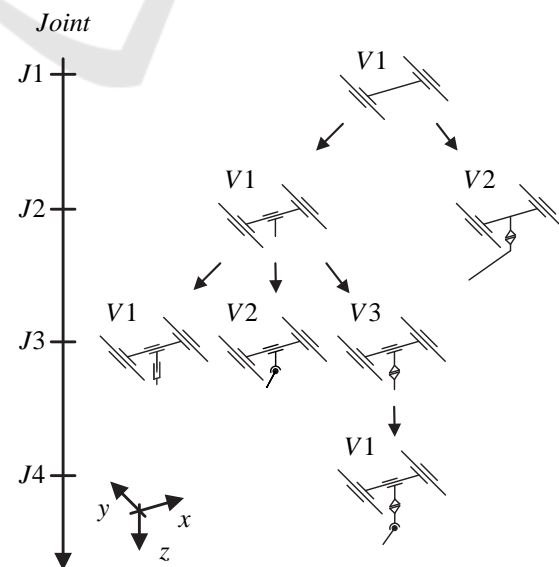

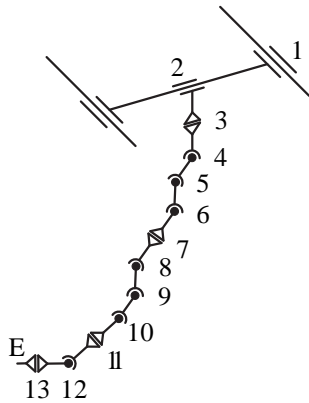Figure 4: Possible configurations of the first four joints.

Figure 5: Tentative topology.

3. $J3V1$ would add a translation in z-direction to span the xyz-volume, but dimensions of currently available technical solutions do not comply with point 2 in section 2. $J3V2$ introduces a rotation around y-axis to span the xyz-volume, but the missing degree of freedom around z-axis for the consecutive robot link limits the dexterity heavily, especially in complex workspaces with obstacles. The rotation of $J3V3$ around the z-axis does not extend the reachable work-space as the other versions, but it leads to a more versatile structure overall.

4. In $J4V1$ the rotation around the x-axis is implemented to span the xyz-volume.

Thus the tentative topology for the positioning mechanism is defined by the joints $J1V1 - J2V1 - J3V3 - J4V1$.

3.2 Dexterous Arm

To fulfill all requirements the minimal degrees of freedom (DoF) is at least 8, where 6 are necessary to reach every point in space in any given orientation and an additional 2 DoF are needed to avoid the a-priori known obstacles. Also, this would only be true if there were no geometric restrictions on the robot design, but the maximum length of the robot links are limited on one hand by the maximum torque in the corresponding joints and on the other hand by the space (described in section 2) that the folded robot is allowed to occupy while passing through the fire doors. Additionally the FCC tunnel cross-section is semi-structured and thus the robot must be able to avoid obstacles which are not known a-priori.

This suggests the introduction of additional DoF, but a general judgment without simulations has, with increasing DoF, already become very tedious. Therefore, a tentative robot topology, with a higher DoF

Table 1: Tentative geometry.

length	[mm]
$l_{1,2}$	*var.*
$l_{2,4}$	288
$l_{4,5}$	500
$l_{5,6}$	500
$l_{6,8}$	400
$l_{8,9}$	400
$l_{9,10}$	400
$l_{10,12}$	200
$l_{12,E}$	100

than the expected optimal solution was set up as a starting point for a subsequent design optimization, see figure 5. The initial geometry is shown in table 1, with the variables $l_{i,j}$ representing the lengths of the manipulator links from joint i to joint j.

The first four joints correspond to the configuration in figure 4. To allow the mechanical structure to fold up in the desired area, joints 5 and 6 were chosen in such a way that they, together with joint 4, form a planar mechanism, which can be folded up easily. The motion plane of this mechanism can be rotated by joint 3. For the consecutive joints 7 to 10, the same planar mechanism was repeated to be able to fold the robot within the very limited space described in section 2. The last three joints 11, 12 and 13 are chosen in such a way that their rotation axes intersect at only one point and thus the solution for orientation and position can be decoupled, which simplifies the optimization problem later on. This configuration of joints also resembles a typical robotic wrist. In section 4 the tentative design will be optimized in order to provide the best manipulator design for the FCC tunnel.

4 DESIGN OPTIMIZATION

In this section the tentative and thus, non-optimal robot topology and geometry of figure 5 and table 1 will be modified, such that the final result provides an optimal and practical feasible solution with respect to certain objectives. The desired goals are minimal production cost and mass, lowest possible energy consumption and high precision. These can be translated into the following optimization objectives:

- Minimize the DoF.
- Minimize the length of each robot link.
- Minimize the motor torques.
- Minimize the error propagation over the mechanical structure.

These objectives need to be constrained in a way, such that the robot is able to reach all desired positions, avoid collisions and can be folded up to fit through the hatches in the fire doors. Similar design optimization problems concerning manipulability measures, error measures and torque minimization are discussed in (Bi and Zhang, 2001) and (Van Henten et al., 2009), but without minimizing the DoF of the mechanical structure.

In section 4.1 a parametrized model of the tentative robot shown in figure 5 and table 1, including kinematics and dynamics, will be defined. The applied collision environment is shown in section 4.2 and the definition of the optimization problem and strategy is shown in section 4.3. The optimized robot design is shown in section 4.6.

4.1 Model

The forward kinematics $\mathbf{f}: \mathbb{R}^{DoF} \rightarrow \mathbb{R}^6$ can be written in the form

$$\mathbf{z} = \mathbf{f}(\mathbf{q}), \tag{1}$$

with the generalized joint coordinates $\mathbf{q} \in \mathbb{R}^{DoF}$ and the Cartesian position and orientation $\mathbf{z} \in \mathbb{R}^6$. An explicit solution for the inverse kinematics is not needed, since it will be taken into account by non-linear equality constraints in the optimization problem.

The dynamic model was found by applying the projection equation (Gattringer, 2011)

$$\sum_{i=1}^{N} \overbrace{\left[\left(\frac{\partial_R \mathbf{v}_{IS}}{\partial \dot{\mathbf{q}}} \right)^T \left(\frac{\partial_R \omega_{IS}}{\partial \dot{\mathbf{q}}} \right)^T \right]_i}^{A_i} \underbrace{\begin{bmatrix} {}_R \dot{\mathbf{p}} + {}_R \widetilde{\omega}_{IR}\, {}_R \mathbf{p} - {}_R \mathbf{f}^e \\ {}_R \dot{\mathbf{L}} + {}_R \widetilde{\omega}_{IR}\, {}_R \mathbf{L} - {}_R \mathbf{M}^e \end{bmatrix}_i}_{B_i} = \mathbf{0}, \tag{2}$$

with the absolute, linear and angular center of mass velocities ${}_R\mathbf{v}_{IS}$ and ${}_R\omega_{IS}$, represented in the body-fixed coordinate frame R, relative to the inertial coordinate frame I. The linear and angular momentum, represented in the body-fixed coordinate frame R

$$\begin{pmatrix} {}_R\mathbf{p} \\ {}_R\mathbf{L} \end{pmatrix} = \begin{bmatrix} m\mathbf{I} & \mathbf{0} \\ \mathbf{0} & {}_R\mathbf{J}^S \end{bmatrix} \begin{pmatrix} {}_R\mathbf{v}_{IS} \\ {}_R\omega_{IS} \end{pmatrix} \tag{3}$$

with the identy matrix $\mathbf{I}$, the mass m and the inertia tensor at center of mass ${}_R\mathbf{J}^S$ in frame R. The acting forces and torques ${}_R\mathbf{f}^e$ and ${}_R\mathbf{M}^e$ on the sub-system and cross product matrix

$$\omega = \begin{pmatrix} \omega_x \\ \omega_y \\ \omega_z \end{pmatrix} \text{ and } \widetilde{\omega} = \begin{bmatrix} 0 & -\omega_z & \omega_y \\ \omega_z & 0 & -\omega_x \\ -\omega_y & \omega_x & 0 \end{bmatrix} \tag{4}$$

The term B_i in (2) is the linear and angular momentum for each sub-system, consisting of motor and link, can be independently expressed with respect to the body-fixed coordinate frame of the respective sub-system. The term A_i transforms the momentum of every sub-system according to the directions of free motion, depending on the mechanical constraints of each joint. Summing up over all N sub-systems finally leads to the equation of movement for the entire robot

$$\mathbf{M}(\dot{\mathbf{q}})\ddot{\mathbf{q}} + \mathbf{g}(\mathbf{q}, \dot{\mathbf{q}}) = \mathbf{Q}, \tag{5}$$

with the mass matrix $\mathbf{M}$, the non-linear term $\mathbf{g}(\mathbf{q}, \dot{\mathbf{q}})$ containing gravitational, centrifugal and coriolis terms and the actuator forces and torques $\mathbf{Q}$.

4.2 Collision Avoidance

The environment of the FCC tunnel cross-sections and the robot links were approximated by convex geometric primitives, here specifically Matlab's AlphaShapes (The MathWorks Inc., 2019), which can be passed to a function to calculate the minimal distance between two convex geometric primitives. The approximation of the FCC environment with cylinders and boxes is indicated by red, dashed lines in figures 6 and 7.
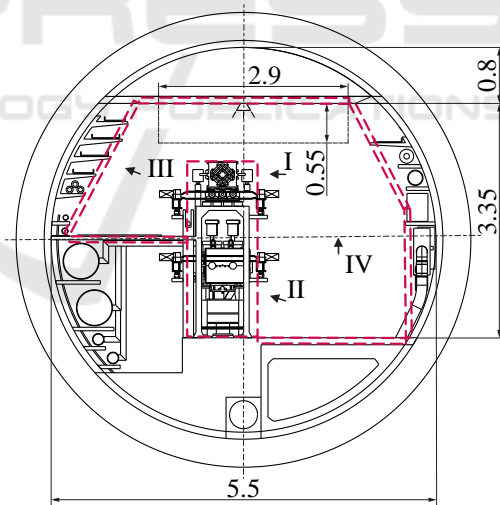

Figure 6: Collision elements FCC-ee.

To reduce the computational cost of the simulation, it was assumed that two consecutive links of a robot can either mechanically not collide or the collision avoidance is included in the upper and lower bounds of the corresponding joint angles. Thus, the n_R serial link robot has to avoid

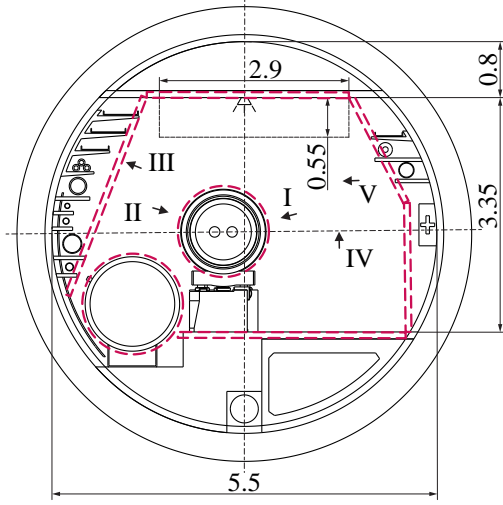$$c_{RR} = \frac{1}{2} \frac{n_R!}{(n_R - 2)!} \tag{6}$$

Figure 7: Collision elements FCC-hh.

possible self collisions and in general

$$c_{RE} = n_R n_E \qquad (7)$$

collisions with the environment. The approximation of the geometry of the manipulator itself can be seen in the final results in figures 11 and 12.

4.3 Problem Formulation

The optimization problem was set up as a non-linear global optimization with non-linear equality and inequality constraints

$$
\begin{aligned}
\min_{\mathbf{x},\,\mathbf{p}_l} \quad & J(\mathbf{x},\,\mathbf{p}_l) \\
\text{s.t.} \quad & \mathbf{f}(\mathbf{x},\,\mathbf{p}_l) - \mathbf{z}_{des} = \mathbf{0} \\
& -\mathbf{c}(\mathbf{x},\,\mathbf{p}_l) \leq \mathbf{0} \\
& \mathbf{ub}(\mathbf{x},\,\mathbf{p}_l) \leq \mathbf{0} \\
& \mathbf{lb}(\mathbf{x},\,\mathbf{p}_l) \leq \mathbf{0}
\end{aligned}
\qquad (8)
$$

with the objective function $J(\mathbf{x},\,\mathbf{p}_l)$ (see section 4.4) and the parameters $\mathbf{x}$ and $\mathbf{p}_l$. The vector $\mathbf{x}$ contains the general coordinates for n_{pos} positions defined in section 2. The vector $\mathbf{p}_l$ contains the geometric parameters, in this case the lengths of the n_{par} robot links. Thus, $\mathbf{x} = \left[\mathbf{q}_1^T, \mathbf{q}_2^T, ..., \mathbf{q}_{n_{pos}}^T\right]^T \in \mathbb{R}^{(n_{DoF} n_{pos}) \times 1}$ and $\mathbf{p}_l \in \mathbb{R}^{n_{par} \times 1}$.

The inverse kinematics is solved with the equality constraint $\mathbf{f}(\mathbf{x}, \mathbf{p}_l) - \mathbf{z}_{des} = \mathbf{0}$, since it is setting the distance between the actual forward kinematics and the desired Cartesian positions and orientations to zero. The vector $\mathbf{c}(\mathbf{x},\,\mathbf{p}_l) \in \mathbb{R}^{(c_{RR}+c_{RE}) \times 1}$ contains the minimal distances according to self-collisions and collisions with the environment. The vectors $\mathbf{ub}(\mathbf{x},\,\mathbf{p}_l)$, $\mathbf{lb}(\mathbf{x},\,\mathbf{p}_l) \in \mathbb{R}^{(n_{DoF} n_{pos}+n_{par}) \times 1}$ are upper and lower boundaries to the joint angles and link lengths.

4.4 Objective Function

As already discussed at the beginning of section 4, the desired objective function should minimize the DoF, the robot link lengths, the torques and the error propagation. This is expressed as linear combination of the multiple objectives

$$
J(\mathbf{x},\,\mathbf{p}_l) = \underbrace{\mathbf{Q}^T(\mathbf{x},\,\mathbf{p}_l)\mathbf{K}_Q \mathbf{Q}(\mathbf{x},\,\mathbf{p}_l)}_{J_1}
$$
$$
+ \underbrace{\mathbf{k}_p^T \arctan(\mathbf{p}_l)}_{J_2} + \underbrace{\mathbf{k}_w^T \mathbf{w}(\mathbf{x},\,\mathbf{p}_l)}_{J_3}. \qquad (9)
$$

In the following sections 4.4.1 to 4.4.3 the effect of each term on the optimization result will be discussed. The vector of torques $\mathbf{Q} \in \mathbb{R}^{(n_{DoF} n_{pos}) \times 1}$ according to (5), is weighted with the diagonal matrix $\mathbf{K}_Q \in \mathbb{R}^{(n_{DoF} n_{pos}) \times (n_{DoF} n_{pos})}$. The second term penalizes the length of the robot links with the weighting factor $\mathbf{k}_p \in \mathbb{R}^{n_{par} \times 1}$ and the third term penalizes the error propagation with the directional kinematic manipulability measure and the corresponding weighting vector $\mathbf{w} = \left[w_1, w_2, ..., w_{n_{pos}}\right]^T$, $\mathbf{k}_w \in \mathbb{R}^{n_{pos} \times 1}$. The directional kinematic manipulability measure (Nait-Chabane et al., 2007) can be written as

$$
w_j = \sum_{i=1}^{3} \left| \mathbf{n}_j^T \mathbf{u}_{j,i} \sigma_{j,i} \right|, \qquad (10)
$$

with the unit vector $\mathbf{n}_j$ representing the direction of interest and the major and minor axes of the manipulability ellipsoid $\sigma_{j,i} \mathbf{u}_{j,i}$ obtained from the singular value decomposition of the geometric Jacobian

$$
\mathbf{J}_j(\mathbf{q}_j, \mathbf{p}_l) = \left[\left(\frac{\partial \mathbf{v}_E}{\partial \dot{\mathbf{q}}} \right)^T \left(\frac{\partial \omega_E}{\partial \dot{\mathbf{q}}} \right)^T \right]^T. \qquad (11)
$$

4.4.1 Effects of Term 1

The first term J_1 minimizes the motor torques of the robot by applying a quadratic objective function. The effects of this function on the optimization result will be shown in a simple example, with the only goal to minimize the torque M of the mechanical structure in figure 8(a). The robot links are assumed massless, thus the only relevant gravitational forces F_G act on joint 2 and the end-effector.

The result of the optimization is shown in figure 8(b). The algorithm changes the link length and joint coordinates in such a way that the mass of the second joint counter-balances the end-effector mass and the resulting torque in joint 1 is $M = 0$.
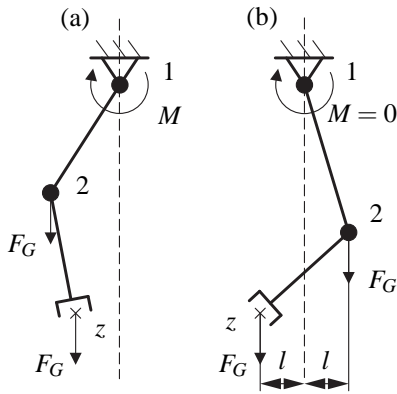
Figure 8: Optimization effects of J_1.

4.4.2 Effects of Term 2

For the following example the goal was to minimize the link lengths and the DoF of the robot, while reaching the desired Cartesian position **z**. With the common approach to minimize parameters by using a quadratic objective function it is possible to minimize the link lengths of the mechanical structure shown in figure 9(a). The result of the optimization with the quadratic objective function is shown in figure 9(b).

It is clear that the optimization converged to an optimum, since the links lie on a straight line from the base to the desired end-effector position. It is also clear that only one DoF would be sufficient to reach this position. Thus, the quadratic objective function is at a minimum when the total length is split up equally over both links.

To minimize the DoF, the distance should not be split up equally, but assigned to only one link, while the other link length will be set to zero. The corresponding joint to this link can then be removed. An objective function $f(x)$ which would lead to the desired behavior needs to satisfy

$$\frac{\partial f(x)}{\partial x} > 0 \qquad (12)$$

to minimize the link length and

$$\frac{\partial^2 f(x)}{\partial x^2} < 0 \qquad (13)$$

to assign the necessary length to only one link and thus minimize the DoF. By setting, e.g.

$$f(x) = \arctan(x), \qquad (14)$$

the above requirements are satisfied. Running the same optimization problem again with the new objective function, the summed up link length is still a minimum and the total length is assigned to only one link since not more than one DoF is necessary to reach the position, see figure 9(c). Thus, the corresponding joint i with $l_i = 0$ can be removed.
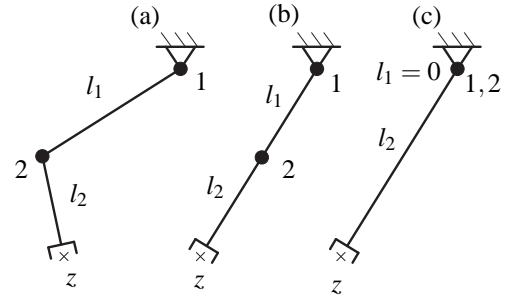
Figure 9: Optimization effects of J_2.

4.4.3 Effects of Term 3

The third term J_3 of the objective function quantifies and minimizes the error propagation in a certain direction of interest. Error propagation describes how certain errors caused by e.g. the elasticity of the gears, backlash or control are being forwarded to the end-effector. Looking at the mapping from joint to Cartesian space via the Jacobian and replacing the small changes in joint angles $\Delta \mathbf{q}$ with an error **e**, the error in Cartesian space is

$$\Delta \mathbf{z}_e = \mathbf{J}(\mathbf{q})\mathbf{e}. \qquad (15)$$

This means that if a robot is in a singularity like the 2-link arm in figure 9(b), the error propagation in direction of the link is 0 and thus, the accuracy only depends on manufacturing tolerances. As a result the optimization algorithm will try to find configurations for which the accuracy is less dependent on the quality of gears or control.

4.5 Model Assumptions

To simplify the optimization of the design in figure 5 and table 1 the system was reduced by omitting the joints 11, 12 and 13 since the orientation can be decoupled from the positions in point 12. Thus, the vector of $n_{DoF} = 10$ generalized coordinates used in the optimization is

$$\mathbf{q}_i = \begin{bmatrix} q_1, \ q_2, \ ..., \ q_{10} \end{bmatrix}_i^T. \qquad (16)$$

To further reduce the complexity of the optimization problem, the linear dependent parameters $l_{6,7}$, $l_{7,8}$ and $l_{10,11}$, $l_{11,12}$ are combined in new parameters $l_{6,8} = l_{6,7} + l_{7,8}$ and $l_{10,12} = l_{10,11} + l_{11,12}$. After the optimization the lengths is split up equally such that $l_{6,7} = l_{7,8} = \frac{l_{6,8}}{2}$ and $l_{10,11} = l_{11,12} = \frac{l_{10,12}}{2}$. Thus, the parameter vector minimizing the $n_{par} = 6$ link lengths is set to

$$\mathbf{p}_l = \begin{bmatrix} l_{4,5}, \ l_{5,6}, \ l_{6,8}, \ l_{8,9}, \ l_{9,10}, \ l_{10,12} \end{bmatrix}^T. \qquad (17)$$
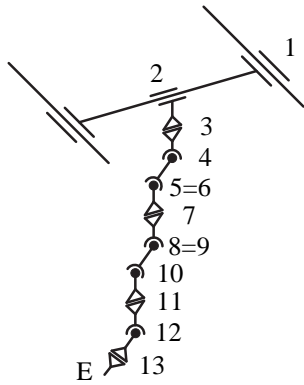
Figure 10: Optimized topology ($DoF = 11$).

Table 2: Optimized geometry.

length	[mm]
$l_{1,2}$	*var.*
$l_{2,4}$	288
$l_{4,5}$	927
$l_{5,6}$	0
$l_{6,8}$	754
$l_{8,9}$	0
$l_{9,10}$	635
$l_{10,12}$	518
$l_{12,E}$	100

The number of different optimization positions is set to $n_{pos} = 5$, as shown in section 2. The necessary motors were chosen by analyzing worst case scenarios and the link masses per meter were designed to withstand these forces.

4.6 Results

The results of the design optimization are visualized in figures 11 and 12, using the geometric primitives described in section 4.2. The robot is visualized in all $n_{pos} = 5$ optimized positions with the optimal lengths of the links. The numeric results for the parameter set $\mathbf{p}_l$ are shown in table 2. The optimal robot link lengths $l_{5,6}$ and $l_{8,9}$ were equal to zero and thus the corresponding joints can be removed and the final DoF was reduced by 2. The resulting topology with 11 DoF is shown in figure 10.

Matlab's *fmincon* function was used as a local optimization solver, in this case applying the interior-point algorithm (Byrd et al., 1999). Furthermore the *GlobalSearch* or *MultiStart* method can be applied to solve the global optimization problem (Ugray et al., 2007) . In a comparison with evolutionary/genetic algorithms, the *GlobalSearch* and *MultiStart* methods lead to better results.
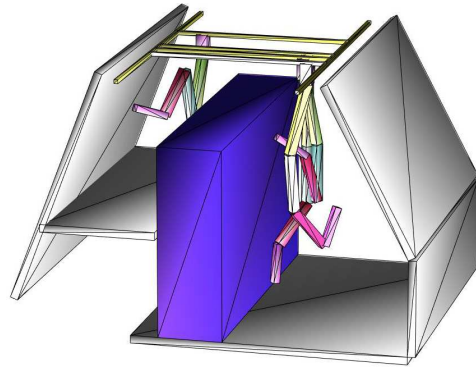

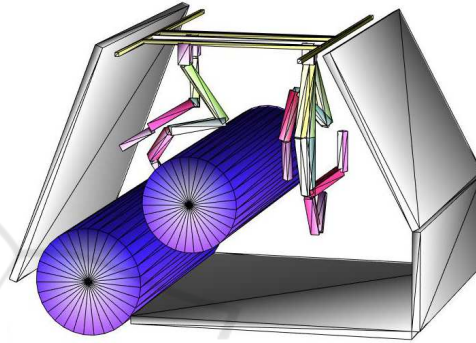Figure 11: Optimization results FCC-ee (collision objects).

Figure 12: Optimization results FCC-hh (collision objects).

5 PROTOTYPE & FUTURE WORK

Based on these findings, the first mechanical structure of the optimized design has been studied, and the results are currently subject to integration in the tunnel cross-sections, within the FCC Integration Board. For the studied scenarios, 24 of these robots will be parked at radiation safe spots around the 100 km long tunnel. The prototype is shown in different scenarios in figures 14 to 15. The goal is to produce the final version of these robots as fully customized solutions specifically for the FCC.

For a proof of concept however, the prototype needs to be simplified in order to reduce the effort of building a fully customized solution. Therefor, only the first 5 joints 1 to 6 in figure 10 (after the optimization joint 5 is identical with joint 6) will be built in-house and for joints 7 to 13 a 6 DoF industrial robot will be used. This industrial manipulator has to fulfill several requirements for seamless integration together with the customized 5 DoF solution:

- Similar topology as joints 7 to 13 in figure 10
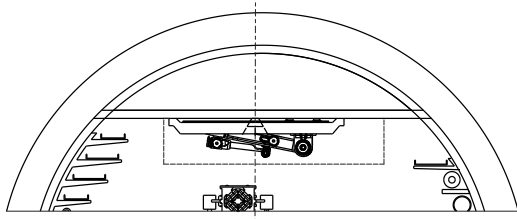- Sufficient payload of at least 10 kg

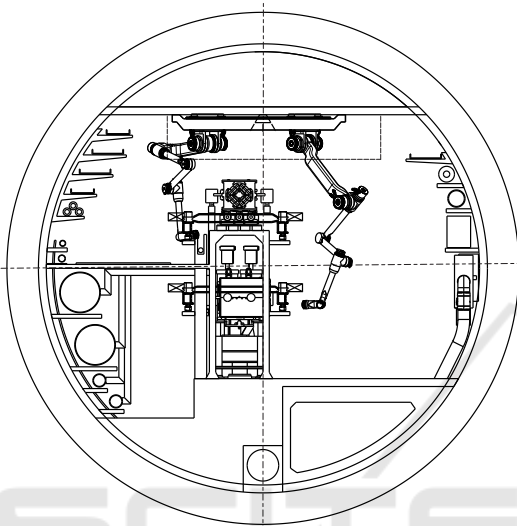Figure 13: Prototype in FCC-ee - folded configuration.
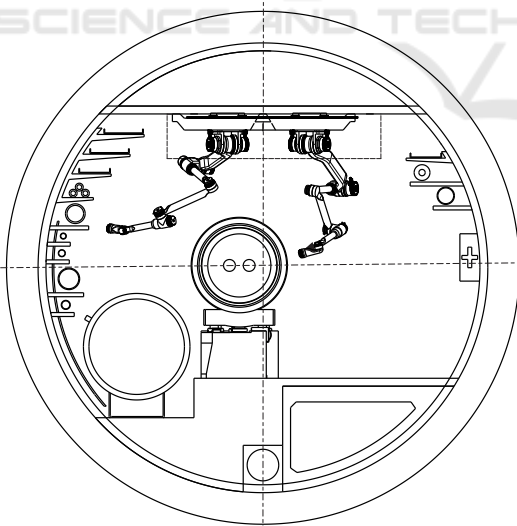

Figure 14: Prototype in FCC-ee cross-section.

Figure 15: Prototype in FCC-hh cross-section.

- 24/48 VDC power supply
- Light weight construction with a total mass less than 40 kg
- An open communication protocol to directly control the motors or an interface to send real-time commands to the provided robot controller

After an extensive research, the 6 DoF collaborative robot UR10e from Universal Robots A/S was found to be the best fit for this application. The next steps will include the design and construction of such a prototype to show proof of concept of the most important and critical tasks in the mock-up tunnels at CERN. The control of the highly redundant system will be implemented in the CERN Robotic Framework (CRF) (Di Castro et al., 2018), a C++ environment similar to ROS (Stanford Artificial Intelligence Laboratory, 2018).

6 CONCLUSION

Once the objective function has been designed, the presented design optimization delivered quantified results for a best fit robot topology with respect to all requirements and constraints. It was possible to minimize the degree of freedom, the link lengths and the torques in each joint. Thus, a optimal topology for the manipulator in the FCC cross-sections was found.

A critical point was to satisfy the different terms J_1, J_2 and J_3 of the objective function. When using different units, like mm and rad the values differed in order of magnitudes and the function needed to be balanced out with the weighting matrices. Furthermore having similar weights for the terms J_1 and J_3 can in some cases cause bad performance, since both terms influence mainly the configuration of the robot. Specifically, if the vector defining the direction of interest for the manipulability measure in 10 is perpendicular to the gravity vector the two terms are working against each other. The optimization time was significantly reduced by providing feasible sets of initial parameters, which were found by running the optimization problem with the objective function $J(\mathbf{x}, \mathbf{p}_l) = 0$. Overall the results of the design optimization are satisfying and fulfilled the requirements.

REFERENCES

Bestmann, P. (2008). The control of the LHC alignment using a robot. Technical report.

Bi, Z. M. and Zhang, W. J. (2001). Concurrent optimal design of modular robotic configuration. *Journal of Robotic Systems*, 18(2):77–87.

Byrd, R. H., Hribar, M. E., and Nocedal, J. (1999). An Interior Point Algorithm for Large-Scale Nonlinear Programming. *SIAM Journal on Optimization*, 9(4):877–900.

Castro, M., Tambutti, M. L. B., Gilardoni, S., Losito, R., Lunghi, G., and Masi, A. (2018). LHC Train Control System for Autonomous Inspections and Measurements.

CDR (2019a). FCC-ee: The Lepton Collider. *The European Physical Journal Special Topics*, 228(2):261–623.

CDR (2019b). FCC-hh: The Hadron Collider. *The European Physical Journal Special Topics*, 228(4):755–1107.

Di Castro, M., Ferre, M., and Masi, A. (2018). CERN-TAURO: A Modular Architecture for Robotic Inspection and Telemanipulation in Harsh and Semi-Structured Environments. *IEEE Access*, 6:37506–37522.

Gattringer, H. (2011). *Starr-elastische Robotersysteme.* Springer, Berlin, Heidelberg.

Holzer, E. B., Dehning, B., Effnger, E., Emery, J., Grishin, V., Hajdu, C., Jackson, S., Kurfuerst, C., Marsili, A., Misiowiec, M., Nagel, M., Busto, E. N. D., Nordt, A., Roderick, C., Sapinski, M., and Zamantzas, C. (2012). Beam Loss Monitoring for LHC Machine Protection. *Physics Procedia*, 37:2055–2062. Proceedings of the 2nd International Conference on Technology and Instrumentation in Particle Physics (TIPP 2011).

M. Bajko, F. B. (2009). Report of the Task Force on the Incident of 19 September 2008 at the LHC. *LHC Project Report 1168*.

Missiaen, D., Steinhagen, R., and Quesnel, J. (2009). The alignment of the LHC. Technical report.

Nait-Chabane, K., Hoppenot, P., and Colle, E. (2007). Directional Manipulability for Motion Coordination of an Assistive Mobile Arm. In *ICINCO*, Angers, France.

Stanford Artificial Intelligence Laboratory (2018). Robotic operating system.

The MathWorks Inc. (2019). Matlab.

Ugray, Z., Lasdon, L., Plummer, J., Glover, F., Kelly, J., and Marti, R. (2007). Scatter Search and Local NLP Solvers: A Multistart Framework for Global Optimization. *INFORMS Journal on Computing*, 19:328–340.

Valentino, G., Aßmann, R., Bruce, R., Redaelli, S., Rossi, A., Sammut, N., and Wollmann, D. (2012). Semiautomatic beam-based LHC collimator alignment. *Phys. Rev. ST Accel. Beams*, 15:051002.

Van Henten, E., Van't Slot, D., Hol, C., and Van Willigenburg, L. (2009). Optimal manipulator design for a cucumber harvesting robot. *Computers and Electronics in Agriculture*, 65(2):247–257.